ACTUATORS

Addressable wireless actuation for multijoint folding robots and devices

Mustafa Boyvat,[1,2]* Je-Sung Koh,[1,2,3]* Robert J. Wood[1,2]*

"Printing" robots and other complex devices through a process of origami-like folding is an emerging and promising manufacturing method due to the inherent simplicity and low cost of folding-based assembly. Folding is used in this class of device to create both complex static structures and flexure-based compliant mechanisms. Dependency on batteries to power these folds with no external wires is a hurdle to giving small-scale folding robots and devices functionality. We demonstrate a battery-free wireless folding method for dynamic multijoint structures, achieving addressable folding motions—both individual and collective folding—using only basic passive electronic components on the device. The method is based on electromagnetic power transmission and resonance selectivity for actuation of resistive shape memory alloy actuators without the need for physical connection or line of sight. We demonstrate the utility of this approach using two folded devices at different sizes using different circuit approaches.

INTRODUCTION

Several nascent subfields in robotics have arisen to address the need for low-cost manufacturing and mass customization. Examples include "printed" robots, pop-up fabrication techniques, and origami-like folding for the design of transformable devices (*1*–*17*). In these areas, folding is the primary mechanism for construction and articulation (e.g., through compliant flexures) (*17*–*28*). Actuation of these folds is a challenge, and achieving folding without hard-wired connections would enable wireless construction and motion of these robots and devices. To date, the most common methods to achieve wireless folding for multiple independent joints involve an on-board battery and microcontroller (*17*, *25*, *28*), whereas efforts to find alternatives are the subject of continuing research (*29*, *30*).

Wireless electromagnetic power transmission is an attractive solution to remove the limitations imposed by discrete batteries, especially for devices operating in enclosed places such as the human body (*31*–*35*). It has been shown that by taking advantage of resonance, extreme performance improvements could be obtained in nonradiative wireless electromagnetic power transmission systems (*36*, *37*). Nevertheless, resonance phenomenon in electromagnetic power transmission systems has mostly focused on power. In contrast, the number of studies considering resonance for selective actuation purposes is still relatively limited (*38*–*43*). Previously, wireless and selective actuation of multiple shape memory alloy (SMA) actuators was shown to be successful, with actuators of millimeter to centimeter sizes exhibiting submillimeter displacements, achieving single and simultaneous excitations (*39*, *40*). It has also been shown that wireless and selective actuation of SMA springs can be used for paper folding applications with a focus on relatively large scales and single actuations at a time (*42*, *43*).

Here, we demonstrate wireless folding of devices with multiple degrees of freedom (DOFs) at millimeter to centimeter scales. The method is based on electromagnetic power transmission and resonance-based selectivity. The method neither requires physical contact nor line of sight, and folding is accomplished using coil SMA actuators that act as the electrical load (*11*, *25*, *44*, *45*). The SMA actuator is widely used and suitable for small-scale robots in terms of high energy density (~2 kJ/kg) with reasonable power range (~1 kW/kg) (*46*). However, SMA is plagued by low efficiency (1 to 5%) due to the thermal nature of the phase change (*46*), therefore limiting the lifetime of battery operation. In this study, the use of a wireless external power source resolves the battery issue for SMA actuators—in this case, the low efficiency of the SMA actuator does not preclude its use.

The receiver circuits use only basic passive electronic components and do not have any on-board power or control. SMA actuators can be activated individually or in groups, ideally independent of whether other actuators are active or not. A diagram illustrating the wireless power transmission concept can be seen in Fig. 1. The method is demonstrated at two different scales (Fig. 2), and associated control circuitry is designed with slightly different approaches. At the larger scale, the resonators are used only for selectivity, whereas a large single coil is used to couple to the external field. Using a single common coupling coil helps the device to be invulnerable to possible nonuniformity in the external field. At a smaller scale, the resonators are used for both selectivity and to couple to the external magnetic field. The approach used in the receiver circuit makes it suitable to drive actuators with low resistances, such as SMA actuators with short lengths and/or high force outputs. The current version of this device, together with all electrical components integrated, weighs 0.8 g.

RESULTS

Circuit design

For the large- and small-scale devices, two slightly different circuitries are used. The circuit diagram and its implementation for the large folding structure can be seen in Figs. 2 and 3. The device is placed in a time-varying magnetic field, and a voltage is induced on the coupling coil according to Faraday's law. The spiral coil can be approximated as a group of circles, and the induced voltage in the phasor domain can be found by the following expression:

$$V_{\text{ind}} = -\sum_{i=1}^{N} j\omega\Phi_i$$

[1]School of Engineering and Applied Sciences, Harvard University, Cambridge, MA 02138, USA. [2]Wyss Institute for Biologically Inspired Engineering, Cambridge, MA 02138, USA. [3]Department of Mechanical Engineering, Ajou University, Suwon 16499, Korea.
*Corresponding author. Email: mboyvat@fas.harvard.edu (M.B.); jskoh@seas.harvard.edu (J.-S.K.); rjwood@seas.harvard.edu (R.J.W.)

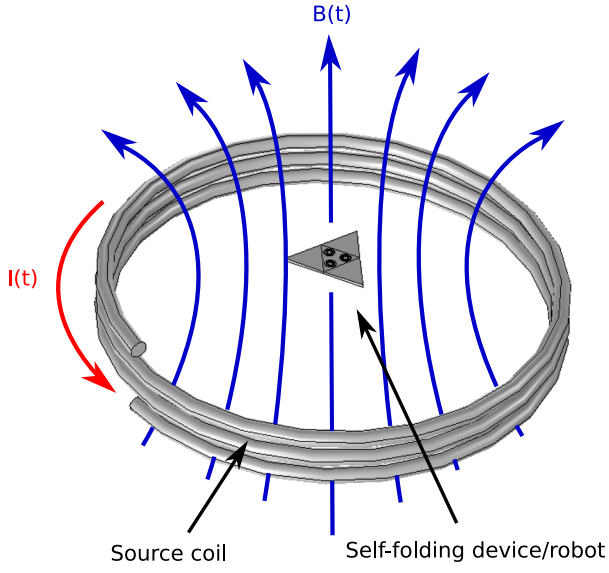

Fig. 1. Illustration of the addressable wireless folding concept. A time-varying magnetic field [$B(t)$] is produced by passing current [$I(t)$] through a source coil. This field induces a voltage on the receiver coil(s) of the purely passive self-folding device/robot and initiates folding at desired joints. Folding at single joints selectively and collective folding at any combination of joints can be realized.

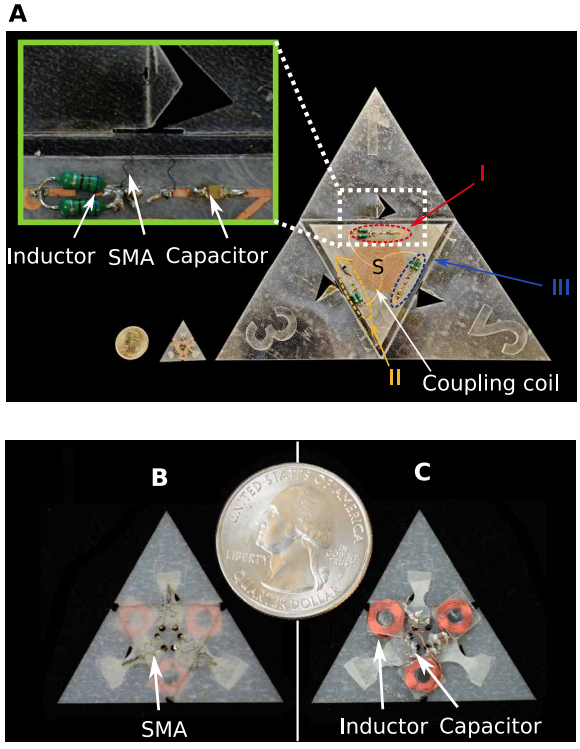

Fig. 2. Self-folding triangular devices at two scales. (**A**) Size comparison of the two devices and the close up view of the electronic components in the larger device. I, II, and III show the circuit parts indicated in Figure 3A. Inductors L_1, L_2, and L_3 (shown in Fig. 3A) are implemented by using two inductors connected in parallel as shown in the inset to increase the current capacity. (**B**) Top view of the smaller device. (**C**) Bottom view of the smaller device. Inductors and capacitors are placed at the bottom of the device. The corresponding circuit diagram can be seen in Fig. 3B.

where N is the number of turns in the spiral, j is the unit imaginary number, $\omega = 2\pi f$, and f is the frequency of the field. Φ_i is the magnetic flux through the surface S_i enclosed by the ith circle and given by

$$\Phi_i = \iint_{S_i} \boldsymbol{B} \cdot d\boldsymbol{A}$$

where $\boldsymbol{B}$ is the magnetic flux density, $d\boldsymbol{A}$ is the differential area vector, and the surface integration is done over S_i. Φ_i and $\boldsymbol{B}$ are also phasor domain expressions.

The coupling coil is connected to a circuit composed of inductors, capacitors, and SMA actuators as resistive elements. Addressing the SMA actuators in the circuit is accomplished by means of inductor-capacitor (LC) resonators. The resonance frequency f_{res} and the impedance Z of a series LC resonator can be calculated using the following equations:

$$f_{res} = \frac{1}{2\pi\sqrt{LC}}$$

$$Z = R + j\omega L + \frac{1}{j\omega C}$$

where R is the resistance, L is the inductance, and C is the capacitance of the resonator. Series LC resonators with different capacitances, therefore with different resonance frequencies, are connected to SMA actuators in series. When the frequency of the applied field is close to the resonance frequency of a series LC resonator, the impedance of the corresponding LC circuit decreases, and the current through the SMA connected to it increases substantially.

In Fig. 3A, L_0 and R_0 are the inductance and resistance, respectively, of the planar spiral coil used to couple to the external magnetic field. V_0 represents the voltage induced by the external field. L_1, L_2, and L_3 are the inductances, and C_1, C_2, and C_3 are the capacitances used to form LC resonators. R_1, R_2, and R_3 are the total resistances due to the corresponding inductors and capacitors, whereas R'_1, R'_2, and R'_3 are the resistances of the SMAs. All the inductances and resistances are kept approximately equal in the LC resonators, and the difference between the resonators is obtained by using different capacitances (C_1, C_2, and C_3). Coupling of L_1, L_2, and L_3 to the external field is neglected. All mutual couplings between L_1, L_2, and L_3 are also neglected. The experimental and analytical frequency responses of the SMAs can be seen in Fig. 4A. Because SMAs are activated by the heat produced by electrical current—proportional to the square of the current passing through them—the square of the current is plotted in Fig. 4A rather than the current itself. During the experimental frequency sweep, the voltage on the SMAs and the voltage induced on a reference coil are measured simultaneously to monitor the external field, and the observed induced voltage is approximately constant over the relevant frequency range. Analytical calculations use the inductance, capacitance, and resistance values obtained by fitting the mathematical model of the circuit to measurements. The numerical values are given in Materials and Methods. Figure 4B shows how strong the maximum current is compared to the currents in the other two resonators. The ratios of the first and the second maximums of the square of the currents through the three resonators are plotted as a measure of selectivity. The frequencies corresponding to the peaks in Fig. 4B are near the resonance frequencies seen in Fig. 4A.

The working principle of the smaller-scale device is similar to the large one. However, in this version, the resonators are used for both

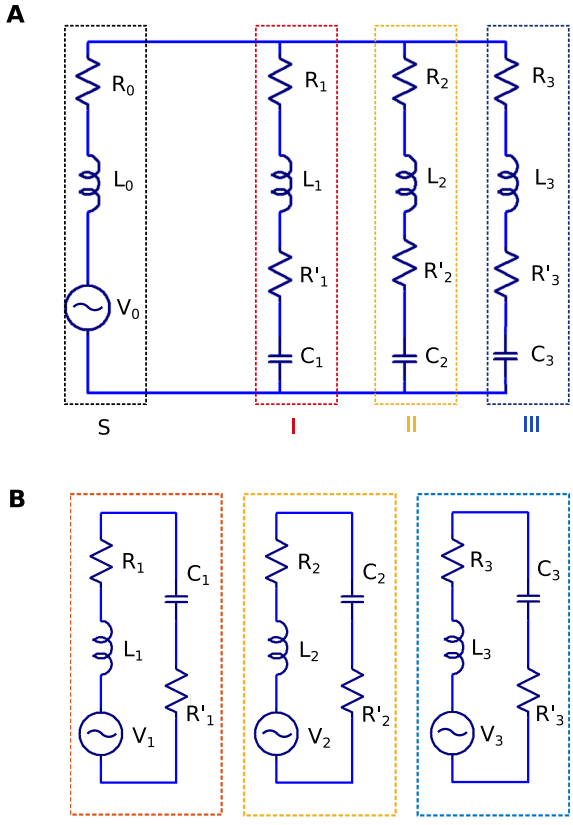

Fig. 3. Circuit diagrams of the wireless actuation electronics in the triangular folding devices. (**A**) The larger device. (**B**) The smaller device.

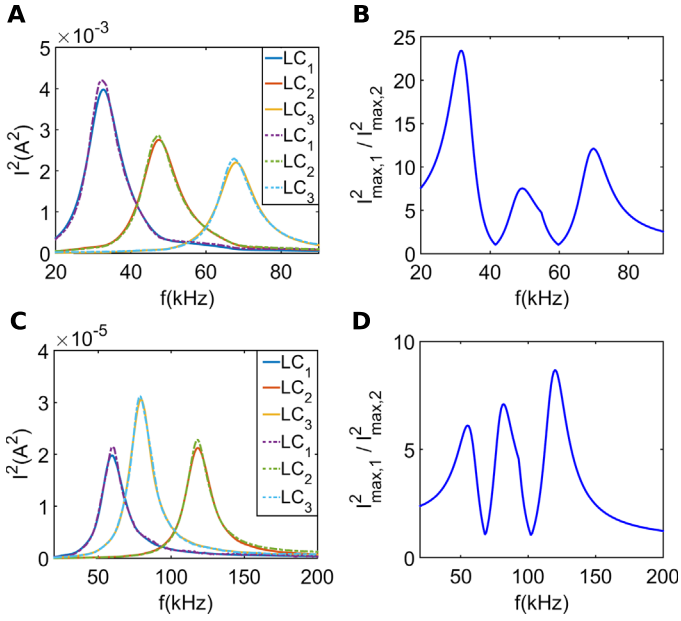

Fig. 4. Characterization of the frequency response of the circuits in the two triangular devices. (**A**) Square of the current through the resonators versus frequency for the circuit in the larger device. Solid lines show analytical calculations and dashed lines show experimental results. (**B**) Ratio of the square of the first maximum current to the square of the second maximum in the resonators as a measure of selectivity for the circuit in the larger device (as calculated using the circuit model shown in Fig. 3). (**C**) Square of the current through the resonators versus frequency for the circuit in the smaller device. Solid lines show analytical calculations, and dashed lines show experimental results. (**D**) Ratio of the square of the first maximum to the square of the second maximum current in the resonators as a measure of selectivity for the circuit in the smaller device.

selectivity and coupling to the external field. The circuit diagram used for the small-scale structure and its implementation can be seen in Figs. 2 and 3. All the resonators are composed of a coil, a capacitor, and an SMA actuator. The numerical values are given in Materials and Methods. At small scales, the small coil surface area puts a considerable limit on received power. This is particularly true when the actuator force stays relatively high and independent of size. In these cases, maximizing received power becomes critical. This maximization can be done by varying the geometry of the coils and/or by choice of operation frequency, considering particular requirements in an application, such as safety regulations, hardware limitations, minimum coil wire thickness (determined by the load), etc. For a given frequency and wire thickness, the received power can be increased by increasing the number of turns in a coil if there is room, keeping the self-resonant frequency of the coil and loss factors, such as proximity effects, in mind. Small SMA actuators with relatively high forces tend to have low resistances and low voltage requirements (in the small-scale device shown here, they are about 2.1 ohms and 0.4 V, respectively). These values can be even lower if an application does not require large strokes, if a device with a smaller size equipped with actuators having relatively high-output forces is desired, or if more efficient shorter SMA actuator designs are used. When these tendencies in coil geometry and actuator resistances are considered, the adopted series connection in the resonators brings some benefits: It is suitable for situations in which load resistances are low compared to coil impedances, and an increase in the number of turns in the receiver coils for a given frequency and wire thickness (remembering loss factors such as proximity effects and self-resonant frequency of coils) is in accordance with selectivity and power transfer capacity. The currents in the resonators with respect to frequency are plotted in Fig. 4C, both experimentally and analytically. Figure 4D shows the selectivity of the resonators in the small device. Although the resonators do not carry equal currents at their peaks due to unequal excitations and the variations in loss terms, sufficiently high selectivity enables proper operation of the device.

Self-folding laminate structure

As a basic multijoint folding device, a tetrahedron-like pattern is designed to test the wirelessly powered self-folding technique. The folding pattern is composed of four identical triangles. Three triangles surround one center triangle and are connected to the three edges of the center triangle via compliant flexures. This design is chosen for simplicity while having several "arms" that can be folded independently to demonstrate the ability to control individual DOFs wirelessly. On the basis of this basic design, the folding structure is constructed as a laminate of rigid and compliant layers using the smart composite microstructure process (*47*). The flexure hinge is a laminated sheet consisting of a single flexible film layer between two rigid composite layers bonded with film adhesives layers, as shown in Fig. 5. The rigid composite layer becomes the faces of the folding structure, and the exposed flexible film acts as compliant flexures. The large difference of bending stiffness between the rigid composite

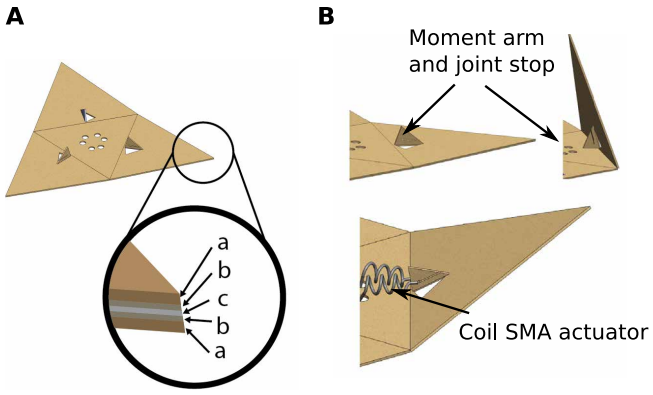

Fig. 5. Folding structure design. (**A**) Three-dimensional rendering of the folding laminate: a, rigid sheet; b, adhesive; c, flexure film. (**B**) Folding joint with a coil SMA actuator with a moment arm that also serves as a fold stop.

sheet and the flexible film makes distinct folding lines. This structure is also widely used as a linkage mechanism in small-scale robots by using folding lines as joint between rigid links (*48*–*51*).

The five layers include rigid outer sheets, film adhesives, and a compliant flexure film, which are laminated by a heat press as shown in Fig. 5A. The rigid sheets are a glass fiber composite (FR4) in the small-scale structure and a thick polyester film (thickness, 250 μm) for the large-scale structure. The adhesive film is a hot mount adhesive (part number 9300712, GBC Inc.), which can be conveniently applied using a thermal laminator. The flexure film is a thin polyester film (thickness, 12.5 μm). The flexure hinge is approximated as a pin joint in parallel with a torsional spring. The spring constant of the flexure is derived from the simple beam bending theory and estimated as $k_\theta = Ewt^3/(12l)$, where E is the Young's modulus of the film material (2.5 GPa for polyester), w is the width, t is the thickness, and l is the gap distance of the flexure hinge. The estimated rotational stiffnesses of the flexure hinges and the maximum required torque are listed in Materials and Methods.

The structure uses a coil SMA actuator at each folding hinge to generate torque for folding. SMA actuators exhibit high energy density [up to about 2 kJ/kg (*46*)], making them suitable for small scales and low-profile structures. In this study, customized coil SMAs are fabricated to achieve a specific force and stroke for the folding structure. Because the required torque to fold the small structure is relatively small, the first design consideration for the coil SMA is the ability to achieve sufficient displacement required for folding. On the other hand, the length of the coil SMA actuators is desired to be short to keep the power requirements low by keeping the resistances low. A coil structure, using a 100-μm-diameter SMA wire (Dynalloy Inc.), is used to trade the high force from the wire for large displacements. The small wire diameter allows the actuator to cool quickly when current is removed. The coil diameter is 1.1 mm, which is made by winding around a 1-mm core. Leveraging a simplified mechanical model of the coil (*45*), an actuator with a single turn, is predicted to achieve a maximum force of 0.3 N and a maximum actuation stroke of 2 mm. The maximum torque that the SMA actuator (the small-scale structure) generates is 0.15 mN·m with a moment arm of 0.5 mm.

To guarantee sufficient stroke and force, we attached a parallel pair of three turn SMA coils producing an actuation distance of 6 mm to the small-scale folding structure, as shown in Fig. 5. A coil SMA actuator for the large-scale structure is designed in a similar way. The wire diameter is 200 μm, and the coil diameter is 1.6 mm, which produces a maximum force of 0.6 N and an actuation stroke of 15 mm. The maximum torque that the SMA actuator (the large-scale structure) generates is 1.2 mN·m with a moment arm of 2 mm. The workspace of the robot is determined by the design of the SMA actuator and the folding pattern. The resulting structure is highly compliant and back-drivable. This may impose challenges for precise control but brings benefits for applications involving the manipulation of delicate structures. A variety of motions types can be obtained by combining several actuators for selective or collective actuations, as demonstrated in this prototype.

The origami folding structure is highly scalable—we are able to make structures in various scales from millimeter to meter scales with an identical folding pattern, although the detailed layer design needs to be tuned depending on the thickness of the structure. For these demonstrations, we built folding structures in two different scales. The larger one has 12-cm folding lines, the smaller one has 1.7-cm folding lines that are seven times smaller than the larger one, and they have the same folding pattern as shown in Fig. 2. However, flexure scaling is adjusted with the thickness of the laminate such that the flexure has the appropriate compliance. The small-scale structure has a 0.4-mm gap distance that is sufficient to avoid interfering during folding of the rigid layer (0.125-mm-thick glass fiber composite), and the large-scale structure has a 0.6-mm gap distance for the 0.25-mm-thick polyester.

Wireless folding

Folding is achieved through heating the SMAs by electrical current. By setting the frequency of the applied external magnetic field close to the resonance frequency of one of the LC resonators, it is possible to activate only the corresponding actuator, and therefore, folding occurs only at the joint where this actuator is connected. To fold at multiple joints simultaneously, the external field needs to contain multiple frequencies. This can be done by either rapidly switching between these frequencies [i.e., by frequency modulation (*39*, *40*)] or superposing the sine waves of these frequencies. Because the actuation of SMA is thermally triggered, one must look into the power dissipated on the SMA actuators to compare these two methods.

In the frequency modulation method, SMA actuators do not continuously carry current (assuming that they carry current only at the associated resonance frequency of that branch of the circuit). If there are n identical SMA actuators to be actuated simultaneously, then the time allocated for an SMA actuator decreases by n times compared to the single continuous excitation, assuming equal time distribution. Therefore, the peak field strength must increase by $\sqrt{n}$ to keep the average power constant (ignoring any variations in actuator power requirements due to the discontinuities in their excitation signals) because the power is proportional to the square of the current. If the superposition method is adopted, then the SMA actuators can carry current continuously at their corresponding resonance frequencies, and individual field strengths remain the same as in a single excitation, but the peak field strength increases to the sum of the peak values in single excitations. Hence, in our experiments, the frequency modulation method is used to keep the peak field requirements low.

Figure 6 illustrates the magnetic field applied to fold all three joints. The frequencies of the applied sine waves are about 32, 48,

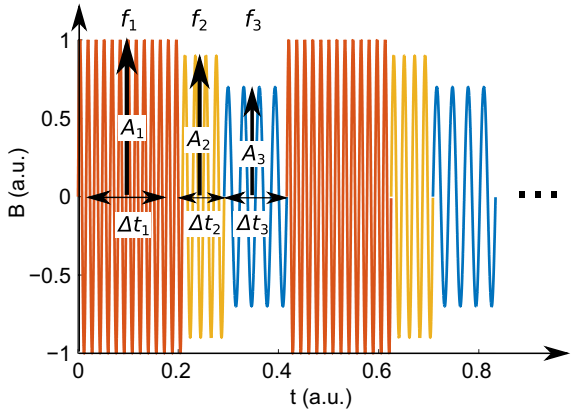

Fig. 6. External magnetic field versus time. Frequency modulation is used to actuate multiple actuators simultaneously.

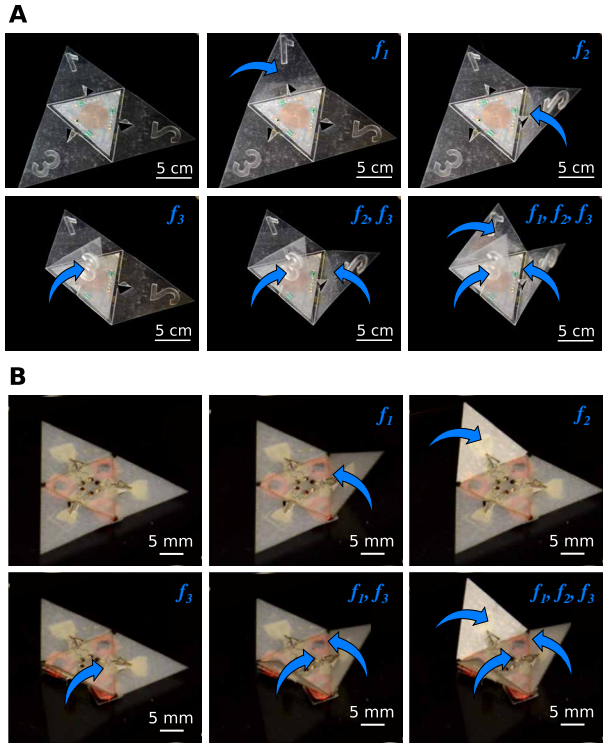

Fig. 7. Wireless folding. (**A**) Wireless folding of the large-scale prototype. Each actuator can be actuated or released individually or collectively. (**B**) Wireless folding of the small-scale structure. The complete device weighs 0.8 g.

and 67 kHz for the large device. In the experiments, signals are applied with 1/600-s periodicity, and both amplitudes (A_1, A_2, and A_3) and the duration of each frequency during a period (Δt_1, Δt_2, and Δt_3) can be controlled. Amplitudes and durations are determined experimentally. By setting the amplitude of any signal to its determined excitation value or to zero, the corresponding SMA can be activated or left inactive, respectively. This enables nearly independent control of folding at all joints as seen in Fig. 7A for the large device. All these cases can be seen in movie S1. The frequency of repeating motions by means of activating and deactivating is limited mainly by the cooling time of the SMAs. The same excitation method is applied to the actuation of the small-scale device using frequencies of about 59, 79, and 113 kHz. The selective and collective folding capabilities of the small device are shown in Fig. 7B and movie S2.

DISCUSSION

This study demonstrates a method for selective wireless folding of multijoint structures achieving all folding combinations but with the absence of on-board power and control. The demonstrations are done at two different size scales and use two different circuit design approaches.

The method is based on wireless electromagnetic power transmission and selective excitation by LC resonances without the need for physical connection or line of sight. At the large scale, the device is sourced by an additional coil coupled to the external magnetic field, whereas at the small scale, the resonators are used both for coupling to the external field and selectivity. The method removes the need for on-board power and control to coordinate actuation for folding [i.e., as in (*19*)]. It enables controlled wireless shape modification in folding-based structures and can provide motion in origami robots by selective folding and unfolding at different joints. These features resolve many problems caused by volumetric limitations in small-scale origami devices/robots, which are not able to carry large batteries or operate for long durations.

Figure 8 shows a battery-free microorigami robotic arm as a demonstration of the methods presented in this paper (see also movies S3 and S4 and figs. S4 and S5). This robotic arm has two origami-like components. One is an adaptive gripper that was introduced in a modular folded laminated robot (*52*), and the other is a spherical six-bar origami pattern that has been used in various origami robots (*45*, *53*). The robotic arm has three coil SMA actuators: two for the arm and one to control the gripper. Selective actuation of the two actuators at each side of two spherical six-bar origami patterns turns the origami robotic arm to the left or right. Activation of both actuators produces a pitching motion. The actuation of the SMA connected to the gripper generates folding at the gripper's flexure joints, resulting in the gripper opening from its normally closed configuration. The arm also includes a permanent magnet on it for positioning and anchoring (*54*). Details about the external magnetic field, electronic circuitry in the device, and the mechanical characteristics of the arm and the gripper can be found in Materials and Methods. A wireless "ship in a bottle" can also be seen in fig. S6 and movie S5 as an additional demonstration. Although it is necessary to redesign the devices and the external excitation considering specifications of particular applications (e.g., size limitations, safety regulations, constraints on the orientation and geometry of transmitter and receiver coils, etc.), we believe that these demonstrations illustrate the viability of collections of wirelessly powered and controlled functional origami robots and devices. One potential use involves origami-based medical devices operating remotely inside the human body without the need for energy storage or control electronics.

Further miniaturization and improvements leading to decreased external magnetic field strength are the subject of future studies that will build on the initial demonstrations presented here. Moreover, modifications that expand to different frequency ranges, increase the working area provided by the external magnetic field setup (see

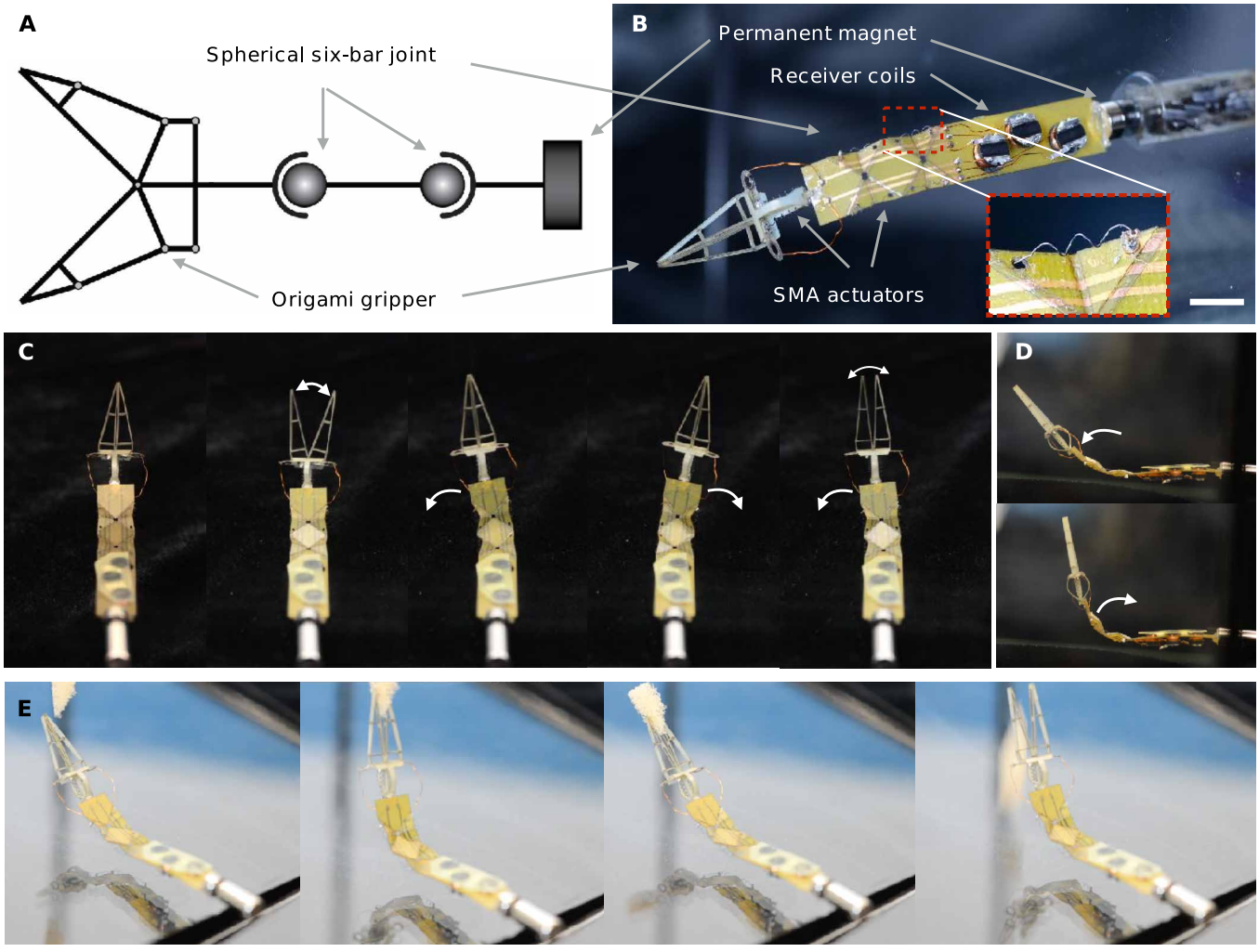

Fig. 8. A battery-free microorigami robotic arm. (**A**) Simplified illustration of the kinematic design and components. (**B**) A working prototype on a glass wall with a permanent magnet for anchoring. The inset figure shows one of the coil SMA actuators attached at the side of the spherical six-bar folding pattern. Scale bar, 1 cm. (**C**) Sequential photos from a movie at various positions by single (left turn, right turn, and gripper open) and multiple actuations (left turn and gripper open together). (**D**) Pitching motion from a lateral perspective. (**E**) Sequential photos from a movie that shows the robotic arm picking up a sponge hanging above and dropping it to the right.

Materials and Methods), and enable orientation-independent operation also deserve further exploration.

MATERIALS AND METHODS

External magnetic field

A planar spiral coil was used as a source coil. Approximate values of turn number, inner radius, and outer radius are 9, 0.94, and 3.3 cm, respectively. How the axial component of the magnetic flux density, B_x, changes with axial distance and radial distance can be seen in fig. S1. This is the component of magnetic flux density inducing voltage on the receiver coils. Figure S2 illustrates the radial and axial variation of B_x in more detail along three selected lines: the axis of the coil and two lines perpendicular to the axis at different distances. The magnetic flux density B_x shown was calculated for a current of 3.5 A and approximating the spiral coil as a combination of circular current loops. The magnetic flux density necessary to actuate the small triangular device is found to be on the order of 0.7 to 0.8 mT by the field calculations and experimental observations. The average magnetic flux density values necessary for the operation of the large device are calculated to be on the order of several milliteslas.

Power considerations

In the larger device, the ratio of the electrical power dissipated on SMA actuators to the total dissipated power in the device is calculated to be between 10 and 20% in the actuation process. In the smaller device, this ratio is between 35 and 50%. The electrical power delivered to SMA actuators in the larger device during actuation is 0.9 to 1.5 W, and it is 84 mW in the smaller device. It is assumed that necessary current values to actuate the SMA actuators are 660 and 200 mA in the larger and smaller device, respectively (www.dynalloy.com).

Circuit details

The values of L_0 and R_0 in the larger device are about 7 μH (kg m^2 s^{-2} A^{-2}) and 3.5 ohms, respectively. The values of L_1, C_1, and $R_{tot,1}$ (total resistance in the resonator 1); L_2, C_2, and $R_{tot,2}$ (total resistance in the resonator 2); and L_3, C_3, and $R_{tot,3}$ (total resistance in the resonator 3) in the larger and smaller devices can be seen in Table 1. The values

Table 1. Values of the components.

	L_1	C_1	$R_{tot,1}$	L_2	C_2	$R_{tot,2}$	L_3	C_3	$R_{tot,3}$
Large scale	232 μH	100 nF	12 ohms	238 μH	46 nF	15 ohms	252 μH	20 nF	16 ohms
Small scale	39 μH	180 nF	4.5 ohms	42 μH	98 nF	4.6 ohms	43 μH	42 nF	5.5 ohms

Table 2. Resonance frequencies and quality factors of the resonators.

	$f_{res,1}$	Q_1	$f_{res,2}$	Q_2	$f_{res,3}$	Q_3
Large scale	33 kHz	4	48 kHz	4.8	71 kHz	7
Small scale	60 kHz	3.3	78 kHz	4.5	118 kHz	5.8

Table 3. Characteristics of the flexure hinge.

	Large scale	Small scale
Torsional stiffness (mN·m/rad)	81.3×10^{-3}	17.2×10^{-3}
Maximum required torque (mN·m)	99×10^{-3}	21×10^{-3}

Table 4. Coil SMA actuator design.

	Large scale	Small scale
Wire diameter (μm)	200	100
Coil diameter (mm)	1.6	1.1
Number of turns	6	3
Maximum stroke (mm)	15	6
Maximum force (N)	0.6	0.3

are obtained by fitting analytical models of the circuits to experimental results. An important term quantifying resonators is the quality factor (Q) because a larger Q means greater selectivity and lower bandwidth, allowing for more channels in a given frequency band. The quality factors (Q) and the resonance frequencies of the resonators can be seen in Table 2. The resonance frequencies are calculated by $1/(2\pi\sqrt{LC})$, and the quality factors are calculated by $(1/R)\cdot\sqrt{L/C}$ for isolated resonators; therefore, they are slightly different from the resonance frequencies of the complete circuit in the larger device and all mutual couplings are ignored. The frequencies used in the actuation of the devices are close to the peaks in the characterization data collected at low power levels (Fig. 4), and the final values of the frequencies used in the actuation were determined experimentally based on the operation of the folding device and the capabilities of our setup at power levels, which are high enough to actuate folding.

In the robotic arm demonstration, commercially available 470-μH inductors with magnetic cores are connected with capacitors and SMA actuators in series, similar to the smaller folding device. The capacitance values in the resonators of the robotic arm are about 2.35, 3.3, and 4.7 nF. The final actuation frequencies of the resonators are found by placing a small nonmagnetic coil in the vicinity of each resonator and observing the induced voltage on the coil by sweeping the frequency of the external field. The approximate external magnetic field frequencies used for actuation are 106 kHz for the gripper and 126 and 151 kHz for the arm. The resistances of the SMA actuators in the arm are about 2.5 ohms, and the resistance of the gripper actuator is measured to be about 2 ohms. Whereas the diameter of the wire used in the arm actuators is 100 μm, the gripper actuator wire has a diameter of 150 μm.

Folding structure details

Figure S3 shows the folding pattern including lines for folding and cutting. Upon actuation, the two-dimensional (2D) structure is folded into a 3D tetrahedron-like structure. Small triangle structures in the outer triangular faces act as moment arms to allow the linear actuators to generate folding torques. This structure is also used as a stop to control the maximum folding angle. Details of the flexure hinges and the SMA actuators in the triangular folding devices are given in Tables 3 and 4. The SMA actuators used in the arm are similar to the actuators in the smaller triangular device. Therefore, similar actuation forces can be assumed in the smaller triangular device. The design of the robotic arm is not optimized for load capacity. The maximum holding force of the origami gripper is about 0.25 N and depends on the object size and shape (*52*). The lifting force of the arm is estimated to be on the order of 7.5 mN from the folding torque of the actuator (0.15 mN·m), and the distance to the gripper is 2 cm.

To generate cut patterns for each layer, we used PopupCAD (*55*, *56*), a software developed to assist in the design of folded composite structures. Using PopupCAD, the detailed cut lines are generated, as shown in figs. S3 and S4. The fold lines have a castellated pattern to minimize off-axis deformation in the flexures (*3*).

SUPPLEMENTARY MATERIALS

robotics.sciencemag.org/cgi/content/full/2/8/eaan1544/DC1
Fig. S1. Magnetic flux density of the source coil.
Fig. S2. Magnetic flux density variation with distance from the coil center.
Fig. S3. Folding structure design.
Fig. S4. Robotic arm design.
Fig. S5. Mechanism of the origami gripper.
Fig. S6. Foldable ship in a bottle.
Movie S1. Wireless folding of the large-scale prototype.
Movie S2. Wireless folding of the small-scale prototype.
Movie S3. A wireless robotic arm and gripper: capabilities.
Movie S4. A wireless robotic arm and gripper: gripping an object and moving.
Movie S5. Wireless ship in a bottle.

REFERENCES AND NOTES

1. J. T. B. Overvelde, J. C. Weaver, C. Hoberman, K. Bertoldi, Rational design of reconfigurable prismatic architected materials. *Nature* **541**, 347–352 (2017).

2. J. T. B. Overvelde, T. A. de Jong, Y. Shevchenko, S. A. Becerra, G. M. Whitesides, J. C. Weaver, C. Hoberman, K. Bertoldi, A three-dimensional actuated origami-inspired transformable metamaterial with multiple degrees of freedom. *Nat. Commun.* **7**, 10929 (2016).
3. P. S. Sreetharan, J. P. Whitney, M. D. Strauss, R. J. Wood, Monolithic fabrication of millimeter-scale machines. *J. Micromech. Microeng.* **22**, 055027 (2012).
4. J. P. Whitney, P. S. Sreetharan, K. Y. Ma, R. J. Wood, Pop-up book MEMS. *J. Micromech. Microeng.* **21**, 115021 (2011).
5. K. Lee, C. W. Chien, B. Lee, A. Lamoureux, M. Shlian, M. Shtein, P. Ku, S. Forrest, Origami solar-tracking concentrator array for planar photovoltaics. *ACS Photonics* **3**, 2134 (2016).
6. A. Lamoureux, K. Lee, M. Shlian, S. R. Forrest, M. Shtein, Dynamic kirigami structures for integrated solar tracking. *Nat. Commun.* **6** 8092 (2015).
7. D. Davis, R. Mailen, J. Genzer, M. D. Dickey, Self-folding of polymer sheets using mi- crowaves and graphene ink. *RSC Adv.* **5**, 89254–89261 (2015).
8. Y. Liu, M. Miskiewicz, M. J. Escuti, J. Genzer, M. D. Dickey, Three-dimensional folding of pre-strained polymer sheets *via* absorption of laser light. *J. Appl. Phys.* **115**, 204911 (2014).
9. G. J. Hayes, Y. Liu, J. Genzer, G. Lazzi, M. D. Dickey, Self-folding origami microstrip antennas. *IEEE Trans. Antennas Propag.* **62**, 5416–5419 (2014).
10. J. B. Gafford, S. B. Kesner, R. J. Wood, C. J. Walsh, Microsurgical devices by pop-up book mems, in *Proceedings of the ASME 2013 International Design Engineering Technical Conferences and Computers and Information in Engineering Conference IDETC/CIE* (American Society of Mechanical Engineers, 2013), pp. V06AT07A011–V06AT07A011.
11. K. Zhang, C. Qiu, J. S. Dai, Helical kirigami-enabled centimeter-scale worm robot with shape-memory-alloy linear actuators. *J. Mech. Robot.* **7**, 021014 (2015).
12. H. Shigemune, S. Maeda, Y. Hara, U. Koike, S. Hashimoto, Kirigami robot: Making paper robot using desktop cutting plotter and inkjet printer, in *IEEE/RSJ International Conference on Intelligent Robots and Systems (IROS)* (IEEE, 2015), pp. 1091–1096.
13. H. Shigemune, S. Maeda, Y. Hara, N. Hosoya, S. Hashimoto, Origami robot: A self-folding paper robot with electrothermal actuator created by printing. *IEEE/ASME Trans. Mechatronics* **21**, 2746–2754 (2016).
14. E. Hawkes, B. An, N. M. Benbernou, H. Tanaka, S. Kim, E. D. Demaine, D. Rus, R. J. Wood, Programmable matter by folding. *Proc. Natl. Acad. Sci. U.S.A.* **107**, 12441–12445 (2010).
15. A. M. Hoover, R. S. Fearing, Fast scale prototyping for folded millirobots, in *IEEE International Conference on Robotics and Automation (ICRA)* (IEEE, 2008), pp. 886–892.
16. A. M. Mehta, D. Rus, An end-to-end system for designing mechanical structures for print-and-fold robots, in *IEEE International Conference on Robotics and Automation (ICRA)* (IEEE, 2014), pp. 1460–1465.
17. C. D. Onal, M. T. Tolley, R. J. Wood, D. Rus, Origami-inspired printed robots. *IEEE/ASME Trans. Mechatronics* **20**, 2214–2221 (2015).
18. M. T. Tolley, S. M. Felton, S. Miyashita, D. Aukes, D. Rus, R. J. Wood, Self-folding origami: Shape memory composites activated by uniform heating. *Smart Mater. Struct.* **23**, 094006 (2014).
19. S. M. Felton, K. P. Becker, D. M. Aukes, R. J. Wood, Self-folding with shape memory composites at the millimeter scale. *J. Micromech. Microeng.* **25**, 085004 (2015).
20. M. T. Tolley, S. M. Felton, S. Miyashita, L. Xu, B. Shin, M. Zhou D. Rus, R. J. Wood, Self-folding shape memory laminates for automated fabrication, in *IEEE/RSJ International Conference on Intelligent Robots and Systems (IROS)* (IEEE, 2013), pp. 4931–4936.
21. X. Sun, S. M. Felton, R. Niiyama, R. J. Wood, S. Kim, Self-folding and self-actuating robots: A pneumatic approach, in *IEEE International Conference on Robotics and Automation (ICRA)* (IEEE, 2015), pp. 3160–3165.
22. B. Shin, S. M. Felton, M. T. Tolley, R. J. Wood, Self-assembling sensors for printable machines, in *IEEE International Conference on Robotics and Automation (ICRA)* (IEEE, 2014), pp. 4417–4422.
23. C. D. Onal, R. J. Wood, D. Rus, Towards printable robotics: Origami-inspired planar fabrication of three-dimensional mechanisms, in *IEEE International Conference on Robotics and Automation (ICRA)* (IEEE, 2011), pp. 4608–4613.
24. D. Lee, S. Kim, Y.-L. Park, R. J. Wood, Design of centimeter-scale inchworm robots with bidirectional claws, in *IEEE International Conference on Robotics and Automation (ICRA)* (IEEE, 2011), pp. 3197–3204.
25. S. M. Felton, M. T. Tolley, C. D. Onal, D. Rus, R. J. Wood, Robot self-assembly by folding: A printed inchworm robot, in *IEEE International Conference on Robotics and Automation (ICRA)* (IEEE, 2013).
26. S. M. Felton, M. T. Tolley, B. Shin, C. D. Onal, E. D. Demaine, D. Rus, R. J. Wood, Self-folding with shape memory composites. *Soft Matter* **9**, 7688–7694 (2013).
27. Z. Zhakypov, M. Falahi, M. Shah, J. Paik, The design and control of the multi-modal locomotion origami robot, Tribot, in *IEEE/RSJ International Conference on Intelligent Robots and Systems (IROS)* (IEEE, 2015), pp. 4349–4355.
28. S. Felton, M. Tolley, E. Demaine, D. Rus, R. Wood, A method for building self-folding machines. *Science* **345**, 644–646 (2014).
29. Y. Mao, K. Yu, M. S. Isakov, J. Wu, M. L. Dunn, H. J. Qi, Sequential self-folding structures by 3d printed digital shape memory polymers. *Sci. Rep.* **5**, 13616 (2015).
30. Y. Liu, B. Shaw, M. D. Dickey, J. Genzer, Sequential self-folding of polymer sheets. *Sci. Adv.* **3**, e1602417 (2017).
31. G. Pan, L. Wang, Swallowable wireless capsule endoscopy: Progress and technical challenges. *Gastroenterol. Res. Pract.* **2012**, 841691 (2012).
32. D. Pivonka, A. Yakovlev, A. S. Y. Poon, T. Meng, A mm-sized wirelessly powered and remotely controlled locomotive implant. *IEEE Trans. Biomed. Circuits Syst.* **6**, 523–532 (2012).
33. J. Ho, S. Kim, A. S. Y. Poon, Midfield wireless powering for implantable systems. *Proc. IEEE* **101**, 1369–1378 (2013).
34. J. S. Ho, A. J. Yeh, E. Neofytou, S. Kim, Y. Tanabe, B. Patlolla, R. E. Beygui, A. S. Y. Poon, Wireless power transfer to deep-tissue microimplants. *Proc. Natl. Acad. Sci. U.S.A.* **111**, 7974–7979 (2014).
35. M. R. Basar, M. Y. Ahmad, J. Cho, F. Ibrahim, Application of wireless power transmission systems in wireless capsule endoscopy: An overview. *Sensors* **14**, 10929–10951 (2014).
36. A. Karalis, J. Joannopoulos, M. Soljačić, Efficient wireless *non-radiative mid-range* energy transfer. *Ann. Phys. Rehabil. Med.* **323**, 34–48 (2008).
37. A. Kurs, A. Karalis, R. Moffatt, J. D. Joannopoulos, P. Fisher, M. Soljacic, Wireless power transfer via strongly coupled magnetic resonances. *Science* **317**, 83–86 (2007).
38. M. Boyvat, C. Hafner, J. Leuthold, Wireless control and selection of forces and torques—Towards wireless engines. *Sci. Rep.* **4**, 5681 (2014).
39. M. M. Ali, K. Takahata, Selective rf wireless control of integrated bulk-micromachined shape-memory-alloy actuators and its microfluidic application, in *IEEE 24th International Conference on Micro Electro Mechanical Systems (MEMS)* (IEEE, 2011), pp. 1269–1272.
40. M. M. Ali, K. Takahata, Wireless microfluidic control with integrated shape-memory-alloy actuators operated by field frequency modulation. *J. Micromech. Microeng.* **21**, 075005 (2011).
41. X. Chen, L. Song, B. Assadsangabi, J. Fang, M. S. M. Ali, K. Takahata, Wirelessly ad- dressable heater array for centrifugal microfluidics and escherichia coli sterilization, in *35th Annual International Conference of the IEEE Engineering in Medicine and Biology Society (EMBC)* (IEEE, 2013), pp. 5505–5508.
42. K. Zhu, H. Nii, O. N. N. Fernando, A. D. Cheok, Selective inductive powering in hardware-based paper computing, in *Lecture Notes in Computer Science* (Springer, 2011), vol. 7040, pp. 340–344.
43. K. Zhu, H. Nii, O. N. N. Fernando, A. D. Cheok, Selective inductive powering system for paper computing, in *Proceedings of the 8th International Conference on Advances in Computer Entertainment Technology (ACE)* (ACM, 2011), p. 59.
44. J.-S. Koh, K.-J. Cho, Omegabot: Biomimetic inchworm robot using SMA coil actuator and smart composite microstructures (SCM), in *IEEE International Conference on Robotics and Biomimetics (ROBIO)* (IEEE, 2009), pp. 1154–1159.
45. J.-S. Koh, K.-J. Cho, Omega-shaped inchworm-inspired crawling robot with large-index-and-pitch (LIP) SMA spring actuators. *IEEE/ASME Trans. Mechatronics* **18**, 419–429 (2013).
46. J. D. W. Madden, N. A. Vandesteeg, P. A. Anquetil, P. G. A. Madden, A. Takshi, R. Z. Pytel, S. R. Lafontaine, P. A. Wieringa, I. W. Hunter, Artificial muscle technology: Physical principles and naval prospects. *IEEE J. Ocean. Eng.* **29**, 706–728 (2004).
47. R. J. Wood, S. Avadhanula, R. Sahai, E. Steltz, R. S. Fearing, Microrobot design using fiber reinforced composites. *J. Mech. Des.* **130**, 052304 (2008).
48. R. J. Wood, The first takeoff of a biologically inspired at-scale robotic insect. *IEEE Trans. Robot.* **24**, 341–347 (2008).
49. K. Y. Ma, P. Chirarattananon, S. B. Fuller, R. J. Wood, Controlled flight of a biologically inspired, insect-scale robot. *Science* **340**, 603–607 (2013).
50. J.-S. Koh, E. Yang, G.-P. Jung, S.-P. Jung, J. H. Son, S.-I. Lee, P. G. Jablonski, R. J. Wood, H.-Y. Kim, K.-J. Cho, Jumping on water: Surface tension–dominated jumping of water striders and robotic insects. *Science* **349**, 517–521 (2015).
51. M. A. Graule, P. Chirarattananon, S. B. Fuller, N. T. Jafferis, K. Y. Ma, M. Spenko, R. Kornbluh, R. J. Wood, Perching and takeoff of a robotic insect on overhangs using switchable electrostatic adhesion. *Science* **352**, 978–982 (2016).
52. J.-s. Koh, D. M. Aukes, B. Araki, S. Pohorecky, Y. Mulgaonkar, M. T. Tolley, V. Kumar, D. Rus, R. J. Wood, A modular folded laminate robot capable of multi modal locomotion, in *Conference on International Symposium on Experimental Robotics (ISER)* (Springer 2016), pp. 59–70.
53. M. Salerno, K. Zhang, A. Menciassi, J. S. Dai, A novel 4-dof origami grasper with an SMA-actuation system for minimally invasive surgery. *IEEE Trans. Robot.* **32**, 484–498 (2016).
54. G. Tortora, T. Ranzani, I. De Falco, P. Dario, A. Menciassi, A miniature robot for retraction tasks under vision assistance in minimally invasive surgery. *Robotics* **3**, 70–82 (2014).

55. D. M. Aukes, B. Goldberg, M. R. Cutkosky, R. J. Wood, An analytic framework for developing inherently-manufacturable pop-up laminate devices. *Smart Mater. Struct.* **23**, 094013 (2014).
56. PopupCAD, www.popupcad.org/.

Acknowledgments: We thank B. Goldberg for help in coil fabrication. **Funding:** We are grateful for support from the NSF (award number CCF-1138967) and the Wyss Institute for Biologically Inspired Engineering. In addition, the prototypes were enabled by equipment supported by the ARL Defense University Research Instrumentation Program (DURIP) program (award number W911NF-13-1-0311). Furthermore, M.B. acknowledges the support by the Early Postdoc.Mobility Fellowship from Swiss NSF. **Author contributions:** M.B. and R.J.W. initiated the project. M.B. and J.-S.K. performed the research, and all authors contributed to development of the project and to preparation of the manuscript. **Competing interests:** The authors declare that they have no competing interests. **Data and materials availability:** M.B., J.-S.K., or R.J.W. may be contacted for additional information.

Submitted 18 March 2017
Accepted 15 June 2017
Published 19 July 2017
10.1126/scirobotics.aan1544

Citation: M. Boyvat, J.-S. Koh, R. J. Wood, Addressable wireless actuation for multijoint folding robots and devices. *Sci. Robot.* **2**, eaan1544 (2017).

Science Robotics

Addressable wireless actuation for multijoint folding robots and devices

Mustafa Boyvat, Je-Sung Koh, and Robert J. Wood

Sci. Robot. **2** (8), eaan1544. DOI: 10.1126/scirobotics.aan1544

Science Robotics (ISSN 2470-9476) is published by the American Association for the Advancement of Science. 1200 New York Avenue NW, Washington, DC 20005. The title *Science Robotics* is a registered trademark of AAAS.